

Neutral Pions and η Mesons as Probes of the Hadronic Fireball in Nucleus–Nucleus Collisions around $1A$ GeV

R. Auerbeck^{1,*}, R. Holzmann¹, V. Metag², R. S. Simon¹

¹*Gesellschaft für Schwerionenforschung, D-64291 Darmstadt, Germany*

²*II. Physikalisches Institut, Universität Gießen, D-35392 Gießen, Germany*

(June 8, 2022)

Abstract

Chemical and thermal freeze-out of the hadronic fireball formed in symmetric collisions of light, intermediate-mass, and heavy nuclei at beam energies between $0.8A$ GeV and $2.0A$ GeV are discussed in terms of an equilibrated, isospin-symmetric ideal hadron gas with grand-canonical baryon-number conservation. For each collision system the baryochemical potential μ_B and the chemical freeze-out temperature T_c are deduced from the inclusive π^0 and η yields which are augmented by interpolated data on deuteron production. With increasing beam energy μ_B drops from 800 MeV to 650 MeV, while T_c rises from 55 MeV to 90 MeV. For given beam energy μ_B grows with system size, whereas T_c remains constant. The centrality dependence of the freeze-out parameters is weak as exemplified by the system Au + Au at $0.8A$ GeV. For the highest beam energies the fraction of nucleons excited to resonance states reaches freeze-out values of nearly 15%, suggesting resonance densities close to normal nuclear density at maximum compression. In contrast to the particle yields, which convey the status at chemical freeze-out, the shapes of the related transverse-mass spectra do reflect thermal freeze-out. The observed thermal freeze-out temperatures T_{th} are equal to or slightly lower than

T_c , indicative of nearly simultaneous chemical and thermal freeze-out.

PACS numbers: 24.10.Pa, 25.75.-q, 25.75.Dw

I. INTRODUCTION

Relativistic nucleus–nucleus collisions offer the unique possibility to study nuclear matter under the influence of high temperature and pressure. At incident energies around $1A$ GeV the formation of a hot and dense reaction zone, dubbed the fireball, has been verified experimentally [1]. According to model calculations, the compression phase lasts for time spans of $10 - 15$ fm/c and reaches densities of $2 - 3$ times the nuclear ground–state density [2–5]. Simultaneously, temperatures up to ≈ 100 MeV may be achieved and a substantial fraction of the nucleons participating in the collision is excited to heavier, short–lived resonance states which decay predominantly via meson emission [6–8]. Thus the fireball produced in the energy regime of the heavy–ion synchrotron SIS at GSI Darmstadt comprises nucleons, resonances, and mesons.

It is an interesting question to what extent this hadronic system can be described in terms of chemical and thermal equilibrium. In the present paper we address this issue on the basis of inclusive as well as centrality–selected data on π^0 and η –meson production in collisions of nuclei with equal mass number A . Chapter 2 introduces the relevant concepts and gives a brief account of previous studies of the hadronic fireball at SIS energies. The existing systematics of π^0 and η production is reviewed in chapter 3. There we demonstrate that thermal concepts do provide a useful description of the fireball at SIS energies. Our model of an ideal hadron gas in chemical equilibrium is presented in chapter 4. Chapter 5 discusses the results of the thermal analysis. The chemical composition of the fireball at freeze–out is determined, and the consistency of chemical and thermal freeze–out temperatures is addressed. Finally, the freeze–out conditions of hadronic matter as derived for the SIS energy regime are compared to results obtained from similar analyses of particle ratios measured at significantly higher incident energies at the AGS (Brookhaven National Laboratory) and the SPS (CERN).

II. THERMAL CONCEPTS IN NUCLEUS–NUCLEUS COLLISIONS AT SIS ENERGIES

In the initial phase of nucleus–nucleus collisions with incident kinetic energies E_{beam} around $1A$ GeV a system of interacting nucleons, resonances, and mesons is created. The size of the hadronic fireball depends on the masses of target and projectile nucleus and, in addition, on the centrality of the collision. Within the participant–spectator model, the geometrical overlap of the two nuclei determines the number of nucleons A_{part} which are directly involved. The quantity $B = A_{part}$ thus defines the number of baryons in the system. For symmetric collisions and complete stopping the energy available per baryon is $\sqrt{s}/2 - m_N$, with s given by $4m_N^2 + 2m_N E_{beam}$ and m_N denoting the nucleon mass. The initial conditions of the fireball are therefore fixed. In the subsequent time evolution the available energy is transformed into the excitation of thermal and collective degrees of freedom. The energy turns into heat and provides the mass stored in resonance states and mesons at chemical freeze–out. In addition, the energy builds up compression and produces the flow of the expanding matter.

In a simplified picture hadrons cannot escape from the fireball during the high–density phase of the collision. Nucleons, resonances, and mesons are trapped in a cyclic process of generation, absorption, and re–emission, exemplified for nucleons N , π mesons, and Δ resonances by $NN \rightleftharpoons N\Delta \rightleftharpoons NN\pi$. Within this approach hadrons are released only with the onset of the expansion phase, when mesons and baryons decouple due to the decreasing matter density. Moments in the expansion process when certain degrees of freedom of the system no longer participate in the interaction provide landmarks in the time evolution. One has to distinguish between chemical and thermal freeze–out which – in the limit of sudden freeze–out – correspond to those moments in time when the relative abundances of the particle species or their momentum distributions stop to change. While only inelastic collisions involving the short–range nuclear force can alter the relative particle yields, the momentum distributions of the particles are governed by the larger total interaction

cross sections. Consequently, thermal freeze-out does not occur before chemical freeze-out. Through the frequent scattering processes of the constituents the system maintains chemical and eventually thermal equilibrium.

It has been shown that at the AGS ($E_{beam} \leq 13.7A$ GeV) and the SPS (200A GeV) a large number of hadronic observables, including strange-particle yields, is in quite good agreement with such an equilibrium scenario [9–12]. At the much lower SIS energies, however, only a very limited variety of hadron species is produced with significant yields. Therefore, in contrast to the situation at AGS and SPS energies, the number of observables which may reflect the chemical or thermal freeze-out is comparable to the number of free parameters in common thermal models. Nevertheless, several analyses have been performed to check for consistency between data and thermal-model predictions also at SIS energies. Midrapidity transverse-momentum spectra of charged pions, protons, and deuterons measured in central Ni + Ni collisions at 1.06A, 1.45A, and 1.93A GeV were observed to be consistent with thermal equilibrium if, in addition, collective radial flow was taken into account [13]. For the same reactions also chemical equilibrium has been claimed with close agreement between the chemical freeze-out temperatures and the temperatures derived from the particle spectra. Recently, Cleymans et al. have extended the thermal analysis at SIS energies to comprise also the strange mesons K^+ and K^- . In their systematic study of central collisions of Ni + Ni and Au + Au based on a model with canonical strangeness conservation [14,15] the yields of protons, deuterons, charged pions, and K mesons were found to agree with chemical equilibrium at freeze-out. Failure of their analysis to also accommodate the η meson within this common freeze-out picture [15] may be attributed to the use of extrapolated η yields.

III. EVIDENCE FOR THERMAL BEHAVIOR FROM MESON YIELDS AND SPECTRA

Pions and η mesons are the most abundantly produced mesons at SIS energies. While the pionic degree of freedom is also covered by the spectroscopy of the charged members

of the isospin multiplet, it is only through γ -ray spectroscopy that the η meson becomes observable in nucleus–nucleus collisions. The two neutral mesons π^0 and η can both be identified by a two-photon invariant–mass analysis of coincident photon pairs. Using the Two–Arm Photon Spectrometer, the TAPS collaboration performed a series of systematic meson–production experiments covering incident energies from $0.2A$ GeV to $2.0A$ GeV. These measurements have established an extended data base for π^0 and η production in light (C + C), intermediate–mass (Ar, Ca + Ca), and heavy symmetric systems (Ni + Ni, Kr + Zr, Au + Au) [16–23].

The primary information for the present discussion is provided by the inclusive meson yields. They have been determined within narrow rapidity intervals around midrapidity. For a consistent treatment the data of the various systems are extrapolated to the full solid angle assuming an isotropic source at midrapidity. Fig. 1 shows the resulting average inclusive meson multiplicities $\langle M \rangle$, normalized to the average number of participating baryons $\langle B \rangle$, as a function of the energy available per baryon divided by the corresponding meson mass. Except for the system Au + Au at $0.8A$ GeV [16] and the systems Au + Au and Kr + Zr at $1.0A$ GeV (see table I), where $\langle B \rangle$ has been determined experimentally, we calculate $\langle B \rangle$ from the geometrical overlap of two colliding sharp spheres which gives $\langle B \rangle = A/2$ in case of collision partners with equal mass number A . A steep rise of the normalized meson ratios with increasing energy is observed. In addition, a weaker dependence on the size of the collision system is visible with the clear tendency towards smaller inclusive yields in the heavier systems. The same trends have also been observed in charged–pion production experiments [24,25]. In first approximation all data points fall onto a smooth curve indicating that to a large extent the meson–production probability is determined by the energy available per baryon. This is quite remarkable because π^0 and η production proceed through different baryon resonances: π^0 mesons mainly come from $\Delta(1232)$ –resonance decays, while the heavier η mesons essentially originate from the $N(1535)$ resonance which, at SIS energies, is the only significantly populated baryon resonance with a large decay width into η mesons. The fact that the basic production mechanism is no longer apparent in the observed meson yields

may be interpreted as a first indication for meson emission from an equilibrated source.

The second important result concerns the average transverse momenta $\langle p_t \rangle$ at midrapidity. For the decay of nominal-mass $\Delta(1232)$ and $N(1535)$ resonances one has center-of-mass momenta of 229 MeV/c for π^0 from $\Delta(1232)$ and 182 MeV/c for η from $N(1535)$. For resonances embedded in an isotropic fireball one therefore expects average transverse momenta obeying $\langle p_t \rangle_{\pi^0} > \langle p_t \rangle_{\eta}$. Fig. 2 shows the experimental results as a function of the energy available per baryon. Although the uncertainties for the η data are large compared to those of the π^0 data, the η momenta are clearly higher than the π^0 values, opposite to the expectation. For both mesons the initial rise of $\langle p_t \rangle$ slows down with increasing available energy, indicating possible saturation of the average transverse momentum. We conclude that also with respect to the shapes of the meson spectra the naive expectations based on the production mechanism are not borne out experimentally.

As a third piece of evidence for thermal behavior we mention the transverse-mass spectra of the mesons. At midrapidity the transverse mass m_t of a particle is equivalent to its total energy in the center-of-mass system. Following [26,27], the transverse-mass distribution of particles with mass m emitted isotropically from a thermal source is characterized by a Boltzmann temperature T_B and, at midrapidity, can be approximately described by

$$\frac{1}{m_t^2} \frac{d\sigma}{dm_t} \propto \exp\left(-\frac{m_t}{T_B}\right) \quad \text{with} \quad m_t = \sqrt{m^2 + p_t^2}. \quad (1)$$

In Fig. 3 transverse-mass distributions of π^0 and η mesons are plotted together with fits according to the parametrization given in Eq. 1 for three different systems at incident energies near 2A GeV. Within each reaction the π^0 and η spectra exhibit almost identical inverse-slope parameters T_B which in addition do not change significantly with the mass of the colliding nuclei. In all three systems the π^0 and η intensities roughly coincide for $m_t \geq m_{\eta}$. This indicates that it is the energy required to produce a given transverse mass which determines the relative abundance of the meson species near midrapidity. For low m_t , however, individual differences among the collision systems become apparent. Fig. 3 shows a systematic enhancement over the exponential rise extrapolated from the high- m_t region

if one goes from the light C + C to the heavy Ni + Ni system. The same observations, namely m_t scaling of the π^0 and η intensities and low- m_t enhancement of the π^0 spectrum in heavy systems, have been reported at various energies down to 0.8A GeV and seem to be a general feature of heavy-ion collisions in the SIS-energy regime [16,17,19–21,23]. Possible explanations that have been suggested for the low- m_t enhancement involve pion rescattering through resonance states in the heavier systems [28] and multiple pion decay of heavy resonances [29].

Transverse-mass scaling in the high- m_t region does not prove that the fireball actually has reached chemical equilibrium. The particle spectra of an equilibrated source, however, would follow phase space distributions as observed, at least for vanishing flow.

IV. IDEAL HADRON-GAS MODEL

In our ansatz we assume that at chemical freeze-out the fireball can be described in terms of an ideal, equilibrated hadron gas. As constituents we take into account pions and η mesons, as well as nucleons, deuterons, and all non-strange baryon resonances up to a mass of 1.8 GeV (see table II), which corresponds to $\sqrt{s} - m_N$ at 2A GeV beam energy.

In the grand-canonical description chosen, hadronic matter is characterized by a baryochemical potential μ_B and a temperature T_c . Furthermore, one might consider the isospin of the system. In the present analysis, however, we neglect isospin as an additional degree of freedom, mainly because our data base of π^0 and η yields is insensitive to isospin. Within the isobar model for instance, the π^0 yield amounts to one third of the total pion yield of a heavy-ion collision irrespective of the actual isospin of the projectile-target system. The other important observable at SIS energies, the η meson, does not carry isospin. Thus, only the third observable in our data base, the relative yield of deuterons and nucleons, depends on the isospin.

In the grand-canonical description of a system of noninteracting fermions and bosons the particle-number densities ρ_i are given by integrals over the particle momentum p

$$\rho_i = \frac{g_i}{2\pi^2} \int_0^\infty \frac{p^2 dp}{\exp[(E_i - \mu_B B_i)/T_c] \pm 1}, \quad (2)$$

where g_i is the spin–isospin degeneracy, E_i the total energy in the local restframe, and B_i the baryon number of the particle species i . The form of the denominator in the integrand accounts for the different statistics of fermions and bosons.

Eq. 2 describes an infinitely large system of stable particles and cannot be directly applied to the hadronic fireball in a nucleus–nucleus collision. To account for the fact that the fireball occupies only a finite volume, a surface correction has to be included. We assume a spherical freeze–out volume V_c of radius R_c and obtain a momentum–dependent correction factor $f(pR_c)$ [30,31]

$$f(pR_c) = 1 - \frac{3\pi}{4pR_c} + \frac{1}{(pR_c)^2} \quad (3)$$

in the integrand of Eq. 2. The correction leads to a 30–40% reduction of the individual particle–number densities as compared to infinite nuclear matter. Particle ratios, however, are hardly affected since here the corrections nearly cancel. The freeze–out radius of the system is fixed by baryon number conservation

$$\int_{V_c} \rho_B dV = \langle B \rangle, \quad (4)$$

where the baryon density ρ_B comprises contributions from nucleons, deuterons, and resonances

$$\rho_B = \rho_N + 2\rho_d + \sum_R \rho_R. \quad (5)$$

Given the feedback via Eq. 3, R_c has to be adjusted iteratively. Starting from an ad–hoc initial value, R_c is varied in steps of 0.5 fm in order to fulfill Eq. 4 within the uncertainties of the experimental particle ratios.

The second modification of Eq. 2 is related to the fact that the baryon resonances are unstable particles which do not have a fixed mass but exhibit a broad mass distribution. In contrast to thermal–model analyses of AGS and SPS data, the actual mass distributions

cannot be neglected in the 1A GeV energy regime since here the energy available in the nucleon–nucleon system is comparable to the excitation energy of the baryon resonances. This means that the $\Delta(1232)$ resonance, the lowest of the baryon resonances, is by far the most abundantly populated resonance and that all resonances are populated predominantly in the low–mass tail of their mass distributions. To account for the off–shell behavior of the resonances, the integrand in Eq. 2 is folded with normalized mass distributions $A_i(m)$. These are trivial delta functions for the stable nucleon and deuteron and for the electromagnetically decaying π^0 and η , while the scheme to parametrize the resonance mass distributions has been adopted from [29].

We describe a given resonance mass distribution by a Lorentzian of the form

$$A_R(m) \propto \frac{m^2 \Gamma_R(m)}{(m^2 - m_R^2)^2 + m^2 \Gamma_R^2(m)} , \quad (6)$$

with

$$\int_0^\infty A_R(m) dm = 1 . \quad (7)$$

The characteristic parameters are the nominal resonance mass m_R and the mass–dependent total decay width $\Gamma_R(m)$. As decay modes we take 1π , 2π , and η decay to the nucleon ground state into account. The total decay width at mass m thus is given by

$$\Gamma_R(m) = \Gamma_{1\pi}(m) + \Gamma_{2\pi}(m) + \Gamma_\eta(m) . \quad (8)$$

The 2π decay is described in terms of a one–step process where the resonance decays into a nucleon and an object with angular momentum $l = 0$ and twice the pion mass $m_{2\pi} = 2m_\pi$. The hypothetical di–pion subsequently disintegrates into two pions. With this simplification the 2π decay width can be written in complete analogy to the 1π and η widths. For the mass–dependent partial decay widths $\Gamma_{1\pi,2\pi,\eta}(m)$ we thus obtain

$$\Gamma_{1\pi,2\pi,\eta}(m) = \begin{cases} \Gamma_{1\pi,2\pi,\eta}(m_R) \left(\frac{q}{q_R}\right)^{2l+1} \left(\frac{q_R^2 + \delta^2}{q^2 + \delta^2}\right)^{l+1} & m > m_N + m_{\pi,2\pi,\eta} \quad , \\ 0 & \text{otherwise} \quad . \end{cases} \quad (9)$$

The partial decay widths at $m = m_R$ are listed in Tab. II. The quantity l is the angular momentum of the emitted meson or di-pion, and q is the momentum of the particle in the restframe of the decaying resonance, with q_R denoting the special case of $m = m_R$. The cutoff parameter δ is given by

$$\delta^2 = (m_R - m_N - m_{\pi,2\pi,\eta})^2 + \frac{\Gamma_R^2(m_R)}{4}. \quad (10)$$

Only in the case of the $\Delta(1232)$ resonance we deviate from this prescription, mainly for the sake of consistency. Use of the well-established parameters $\Gamma_R = 110$ MeV and $\delta = 300$ MeV/c determined for this resonance by Koch et al. in a non-relativistic analysis (see [33]) requires an additional term m_R/m on the right-hand side of Eq. 9.

Furthermore, one could consider an excluded-volume correction to take into account the hadron-hadron hard-core repulsion. This means that one would consider a real rather than an ideal hadron gas. An excluded-volume correction, however, does not play a significant role for particle-yield ratios as demonstrated in [12]. Another reason to omit the excluded-volume correction is the fact that chemical freeze-out seems to occur at baryon densities well below the nuclear ground-state density. The system therefore is rather dilute which supports the assumption of an ideal gas of pointlike non-interacting particles.

With the modifications introduced by Eqs. 3 and 6 the particle-number densities of Eq. 2 are given by

$$\rho_i = \frac{g_i}{2\pi^2} \int_0^\infty dp p^2 f(pR_c) \int_0^\infty dm \frac{A_i(m)}{\exp\left[\left(\sqrt{m^2 + p^2} - \mu_B B_i\right)/T_c\right] \pm 1}. \quad (11)$$

Equation 6 employs a mass-dependent width in the resonance-mass distribution. This feature of the model makes it possible to take the actual resonance masses into account if one determines the contributions to the asymptotically observed π^0 and η intensities which originate from resonance decay. The effective branching ratios may deviate significantly from those at the nominal mass m_R . For the latent meson densities $\rho_R^{1\pi,2\pi,\eta}$ represented by a given resonance R one obtains

$$\rho_R^{1\pi,2\pi,\eta} = w \frac{g_R}{2\pi^2} \int_0^\infty dp p^2 f(pR_c) \int_0^\infty dm \frac{\Gamma_{(1\pi,2\pi,\eta)}(m) A_R(m)}{\Gamma_R(m) \exp\left[\left(\sqrt{m^2 + p^2} - \mu_B\right)/T_c\right] + 1} , \quad (12)$$

with $w = 1$ in the case of one-pion or η -meson emission and with $w = 2$ for the two-pion decay. The resonances present at freeze-out also contribute to the asymptotically observed abundance of nucleons. Furthermore, the η meson (lifetime $c\tau = 1.7 \times 10^5$ fm) gives rise to additional π^0 intensity via its $3\pi^0$ and $\pi^+\pi^-\pi^0$ decays with branching ratios of 32% and 23%, respectively.

V. THERMAL-MODEL ANALYSIS

The values for the two parameters of the hadron-gas model – the baryochemical potential μ_B and the temperature T_c – can be derived from any two relative abundances of the constituents. Furthermore, the baryon content of the system has to be known for an assessment of the geometrical size of the fireball. The π^0 and η -meson yields are particularly suited for such an analysis, as these particles unambiguously arise from the fireball. Hence, we base our analysis on the ratios $\langle M_{\pi^0} \rangle / \langle B \rangle$ and $\langle M_\eta \rangle / \langle M_{\pi^0} \rangle$ as compiled in Tabs. I and III. For the sake of redundancy in the analysis we consider the ratio of deuterons to nucleons as additional input information. The knowledge of $\langle M_d \rangle / \langle M_N \rangle$, however, is limited and especially its centrality dependence is difficult to determine experimentally since in non-central collisions it is not trivial to separate deuterons originating from the fireball from those which are emitted by target- or projectile-like spectator remnants.

So far, only a few investigations have addressed deuteron yields in nucleus-nucleus collisions at SIS energies. The inclusive values for $\langle M_d \rangle / \langle M_N \rangle$ given in Tab. I are based on yield ratios of deuterons and protons measured in central collisions of Ni + Ni at 1.06, 1.45, and 1.93A GeV [13] and of Au + Au at 1.0A GeV [35], and on inclusive results obtained for various combinations of light and intermediate-mass nuclei at 0.8A GeV [36]. From these data we parametrized the dependence of $\langle M_d \rangle / \langle M_N \rangle$ on the incident energy and on the

system size. For given system size a linear decrease of $\langle M_d \rangle / \langle M_N \rangle$ with increasing available energy provides a fair description of the existing data. For fixed energy the ratio $\langle M_d \rangle / \langle M_N \rangle$ increases with system size until saturation sets in for heavy systems. The limited number of data points and the uncertainties in the interpolation procedure translate into quite large errors for the ratios $\langle M_d \rangle / \langle M_N \rangle$ (see Tab. I). No attempt has been made to establish an impact–parameter dependence.

In the thermal analysis the three particle ratios are related to the particle–number densities calculated within the thermal model by the following equations:

$$\left(\frac{\langle M_{\pi^0} \rangle}{\langle B \rangle} \right)_{exp} = \frac{1}{\rho_B} \left\{ \frac{1}{3} \left(\rho_\pi + \sum_R \rho_R^{1\pi} + \rho_R^{2\pi} \right) + 1.2 \left(\rho_\eta + \rho_{N(1535)}^\eta \right) \right\}, \quad (13)$$

$$\left(\frac{\langle M_\eta \rangle}{\langle M_{\pi^0} \rangle} \right)_{exp} = \frac{\rho_\eta + \rho_{N(1535)}^\eta}{\frac{1}{3} \left(\rho_\pi + \sum_R \rho_R^{1\pi} + \rho_R^{2\pi} \right) + 1.2 \left(\rho_\eta + \rho_{N(1535)}^\eta \right)}, \quad (14)$$

$$\left(\frac{\langle M_d \rangle}{\langle M_N \rangle} \right)_{exp} = \frac{\rho_d}{\rho_N + \sum_R \rho_R}. \quad (15)$$

Each equation defines a band in the μ_B, T_c –diagram. The widths of these bands are given by the uncertainty of the input values, and for each individual collision system which is characterized by its triplet of particle ratios one obtains the chemical potential and the temperature as coordinates of the common intersection point of the three bands. Provided the experimental uncertainties correspond to Gaussian errors one has a probability of 20% that the true values of the three particle ratios simultaneously fall into the 1σ uncertainty ellipsoid, while this probability rises to 75% for 2σ uncertainty [37]. For a consistent treatment of the full data sample it is therefore necessary to allow for uncertainties in excess of two standard deviations in the input ratios.

The system size also has to be considered as input information. Through baryon conservation expressed in the grand–canonical form of Eq. 4 the baryon number determines the freeze–out radius R_c . For typical values of R_c around 5 fm we find that changes within ± 1 fm

of the final solution hardly affect the numerical values for μ_B and T_c , but substantially alter the freeze-out density ρ_B due to its $1/R_c^3$ dependence. Larger variations up to ± 2 fm may still lead to solutions on the 2σ -level for the particle ratios with changes in μ_B and T_c within $\pm 5\%$, but ρ_B becomes increasingly incompatible with Eq. 4.

The connection between a given particle ratio and the freeze-out parameters μ_B and T_c is illustrated in Fig. 4. A global value of 5 fm for the radius parameter R_c has been chosen to generate the diagram. Curves of constant particle ratio in the μ_B, T_c -plane are referred to as freeze-out lines. Since R_c is fixed, $\langle B \rangle$ varies along the freeze-out lines. The intersection of any two freeze-out lines from different particle ratios thus only describes a physical solution if also the corresponding values of $\langle B \rangle$ overlap. The third freeze-out line then has to intersect within the experimental uncertainty and for the same value of $\langle B \rangle$. In Fig. 5 global values for the triplet of particle ratios have been chosen to demonstrate the variation of the freeze-out lines with the radius parameter.

A. Centrality Dependence of the Freeze-out Parameters

The inclusive particle ratios of the existing data base represent averages over the impact parameter of the collision. Prior to the analysis of the inclusive data we therefore address the centrality dependence of the freeze-out parameters.

The ratios $\langle M_{\pi^0} \rangle / \langle B \rangle$ and $\langle M_\eta \rangle / \langle M_{\pi^0} \rangle$ have been measured as a function of the centrality of the collision in Ar + Ca [21] and Au + Au [16], both at 0.8A GeV. While in the intermediate-mass Ar + Ca system the meson multiplicities per participant nucleon essentially do not depend on the impact parameter, a clear effect is observed in the heavy system Au + Au. From peripheral ($\langle B \rangle = 40 \pm 10$) to central collisions ($\langle B \rangle = 345 \pm 25$), the neutral-pion multiplicity per participant nucleon $\langle M_{\pi^0} \rangle / \langle B \rangle$ increases by a factor of about 1.6, while simultaneously the η -meson multiplicity per participant nucleon $\langle M_\eta \rangle / \langle B \rangle$ increases by a factor of 3.6 (see Tab. III). The enhancement of the η -meson production in central collisions has been attributed to secondary reactions involving resonances as inter-

mediate energy storage [16]. This interpretation is particularly relevant for the large system size and the subthreshold incident energy of the measurement and indicates that dynamical effects may still be visible in these Au + Au collisions.

Fig. 6 illustrates the thermal analysis of Au + Au for peripheral, semicentral, and central collisions. Shown are the three bands in the μ_B, T_c -plane corresponding to the three particle ratios for 1σ and 2σ uncertainties. It is important to understand the correlations between the particle ratios and the parameters of the thermal model. One observes that in the vicinity of the common intersection point of the bands the ratio $\langle M_{\pi^0} \rangle / \langle B \rangle$ is equally sensitive to μ_B and T_c . Larger values of $\langle M_{\pi^0} \rangle / \langle B \rangle$ mean larger temperatures and smaller chemical potentials of the hadron gas. This reflects the fact that with increasing μ_B the baryon density grows while the density of free pions remains unaffected. The ratio $\langle M_\eta \rangle / \langle M_{\pi^0} \rangle$, on the other hand, is practically only sensitive to T_c . Larger values of $\langle M_\eta \rangle / \langle M_{\pi^0} \rangle$ require larger values for T_c , while μ_B is uncritical. This is due to the fact that producing an η meson or exciting an $N(1535)$ resonance requires more energy and thus a higher temperature than producing a pion or exciting a $\Delta(1232)$ resonance because of the pronounced mass difference between both mesons or both resonances, respectively. The third ratio, $\langle M_d \rangle / \langle M_N \rangle$, derives its sensitivity to μ_B from the difference in baryon number of the two particles, while the temperature dependence is governed by the mass difference between the particles. With increasing baryochemical potential the temperature of the system has to drop in order to maintain a given $\langle M_d \rangle / \langle M_N \rangle$ ratio. It should be noted, however, that the sensitivity of the freeze-out parameters with respect to a variation of $\langle M_d \rangle / \langle M_N \rangle$ is small. Modifying the ratio by as much as $\pm 20\%$ changes the freeze-out parameters by not more than 5%. Nevertheless, $\langle M_d \rangle / \langle M_N \rangle$ provides a useful additional constraint in those cases where the neutral-meson data alone would leave room for large variations in μ_B and T_c .

Fig. 6 shows that in 0.8A GeV Au + Au the experimental particle ratios do define unique sets of μ_B and T_c for each of the three impact parameter selections. The numerical values as determined by χ^2 minimization are summarized in Tab. III. The uncertainties quoted represent 1σ standard deviations and reflect the size of the error ellipse of the μ_B, T_c -pair

at $\chi^2 = \chi_{min}^2 + 1$. Within these uncertainties the baryochemical potential and the chemical freeze-out temperature obtained in the most peripheral and central collisions, respectively, agree with the semicentral values of $\mu_B = 812 \pm 5$ MeV and $T_c = 52 \pm 2$ MeV. The ensuing baryon densities ρ_B relative to the nuclear ground-state density ρ_0 are also given in Tab. III.

In our ansatz we are able to describe the central Au + Au collisions at 0.8A GeV with one common set of freeze-out parameters, see Fig. 7, while Cleymans et al. [15] emphasize that they cannot reproduce the ratio $\langle M_\eta \rangle / \langle M_{\pi^0} \rangle$ within their hadron-gas model for the same system at 1.0A GeV. The present analysis is based on the directly measured ratio $\langle M_\eta \rangle / \langle M_{\pi^0} \rangle$ for experimentally determined values of $\langle B \rangle$, while the authors of ref. [15] have to overcome the difficulty that at 1.0A GeV the ratio $\langle M_\eta \rangle / \langle M_{\pi^0} \rangle$ has not been measured for truly central collisions. They extrapolate $\langle M_\eta \rangle / \langle M_{\pi^0} \rangle$ measured in centrality-biased Au + Au collisions at 1.0A GeV beam energy [17] (c.f. Tab. I) to fully central collisions using the centrality dependence of that ratio measured at 0.8A GeV [16]. It is known [16,24], however, that the dependence of the meson multiplicity on the number of baryons in the fireball is governed by the transverse-mass excess $\langle m_t \rangle - (\sqrt{s} - 2m_N)$, giving rise to a steeper increase of the η multiplicity with centrality in the more subthreshold Au + Au collisions at 0.8A GeV. With their approach Cleymans et al. thus overestimate the $\langle M_\eta \rangle / \langle M_{\pi^0} \rangle$ ratio since at 1.0A GeV the production of η mesons is considerably less subthreshold than at 0.8A GeV. In addition, Cleymans et al. were not aware of the fact that the 1.0A GeV measurement is already centrality-biased, the value of $(1.4 \pm 0.6)\%$ corresponding to $\langle B \rangle = 164 \pm 20$ (c.f. Tab. I). Judging from the full variation of 40% observed for the centrality dependence of $\langle M_\eta \rangle / \langle M_{\pi^0} \rangle$ at 1.0A GeV (see ref. [17]) we obtain $\langle M_\eta \rangle / \langle M_{\pi^0} \rangle = (1.8 \pm 0.7)\%$ for central collisions. Thus, the lower boundary of the 2σ uncertainty band for a revised η/π^0 freeze-out line may reach $T_c = 55$ MeV at $\mu_B = 800$ MeV (see Figs. 4 and 5), well within the 2σ ellipsoid of the intersecting remaining freeze-out lines in the analysis of Cleymans et al. [15].

In summary, no significant centrality dependence of the freeze-out parameters is found for the heavy system Au + Au at 0.8A GeV. For the lighter systems and for beam energies which are less subthreshold for η production a possible dependence on the impact parameter

therefore can be neglected at the present level of accuracy.

B. Results for Inclusive Collisions

Fig. 8 shows the results of the thermal analysis for the lightest, an intermediate-mass, and the heaviest system, both at the lowest and highest beam energy studied. Presented in the μ_B, T_c -plane are the bands defined by the input values $\langle M_{\pi^0} \rangle / \langle B \rangle$, $\langle M_\eta \rangle / \langle M_{\pi^0} \rangle$, and $\langle M_d \rangle / \langle M_N \rangle$. In all cases the three bands overlap and, therefore, define the freeze-out parameters μ_B and T_c in an unambiguous way. Even collision systems with as few participating nucleons as C + C seem to comply with the model-assumption of chemical equilibrium. The results for the full set of inclusive measurements are summarized in Tab. IV. The analysis reveals a systematic reduction of the baryochemical potential from 800 to 650 MeV with increasing beam energy, which is accompanied by an increase of the freeze-out temperature from 55 to 90 MeV. For given beam energy the chemical potential μ_B grows with increasing system size while the freeze-out temperature T_c stays almost constant. These findings agree with results quoted from similar analyses [13–15], although we observe a general trend towards smaller baryochemical potentials and higher temperatures as compared to [14,15].

The freeze-out radius R_c is fixed by the average number of baryons through Eq. 4 and enters the model analysis via the surface correction term. R_c is larger for the heavy target-projectile combinations, but increases less than the trivial $\langle B \rangle^{1/3}$ law, and it decreases with increasing beam energy. The corresponding baryon densities at chemical freeze-out are in general smaller than about half the nuclear ground-state density which is in good agreement with results from other analyses [10,11,13].

C. Chemical Composition of the Fireball

The quantities μ_B and T_c are the two important free parameters of our model. They essentially determine the properties of the fireball. As an example, Fig. 9 shows the chemical composition of the baryon sector at chemical freeze-out as a function of the energy available

in the nucleon–nucleon system. The system size is a further parameter. Light, intermediate–mass, and heavy systems are therefore treated separately in Fig. 9.

Immediately apparent is the pronounced energy dependence of the chemical composition, while for any given incident energy the chemical composition is nearly independent on the size of the system. The fraction of baryons excited to resonance states grows from 2–3% at $0.8A$ GeV beam energy to about 15% around $2.0A$ GeV. The $\Delta(1232)$ resonance is populated most abundantly. The ratio of heavier resonances to the $\Delta(1232)$ resonance, however, increases from about 7% at $0.8A$ GeV to nearly 20% around $2.0A$ GeV, indicative of a more equal population of the resonance spectrum at higher incident energies. As illustrated by the straight lines in Fig. 9, the energy dependence of the individual relative baryon populations is in reasonable agreement with exponential behavior. The slopes of these exponentials are nearly equal for $\Delta(1232)$ and $N(1535)$ and steeper for the summed contributions of the remaining Δ and N resonances.

The baryon composition of the chemical freeze–out state being established it is interesting to extrapolate back to the high–density phase of the collision. Around $2A$ GeV beam energy microscopic model calculations quite consistently give a maximum baryon density of $\rho_{max} \approx 2.5 \rho_0$ and predict a ratio of 0.3 to 0.4 for the ratio of the number of $\Delta(1232)$ resonances at freeze–out to the corresponding number at maximum compression [29,38]. Using this information together with an allowance for contributions from higher resonances, one obtains a value of $0.4 \rho_{max} \approx \rho_0$ for the maximum resonance density in the collisions at $1.9A$ and $2.0A$ GeV, see Fig. 9. Although the density of baryon resonances only amounts to about 40% of the total baryon density, resonance–resonance interactions might take place. Hadronic matter in that state has been referred to as resonance matter [6,8].

Concerning the meson sector of the freeze–out state, an important observation is that a sizeable fraction of the mesons are present as free mesons in chemical equilibrium with the baryons. This is immediately apparent, if one compares the population of $\Delta(1232)$ and $N(1535)$ resonances with the π^0 and η multiplicities observed asymptotically (see Tab. I). For a quantitative discussion, we plot in Fig. 10 the fraction of free mesons and the fraction

of mesons bound in resonances at freeze-out as a function of the energy available in the nucleon–nucleon system, again differentiating between light, intermediate–mass, and heavy systems. The relative contributions to the final–state pion yields reveal a moderate energy dependence, the fraction of free pions decreasing from about 65% at 0.8A GeV beam energy to about 55% at 2.0A GeV. Pions from the $\Delta(1232)$ resonance behave in a complementary way, as expected, with contributions of about 30% at 0.8A GeV and about 40% at 2.0A GeV. The remaining intensity can be attributed to heavier resonances which, according to their higher mass, give rise to a steeper energy dependence than exhibited by pions from $\Delta(1232)$ –resonance decays. For η mesons resonance decay after chemical freeze-out is unimportant. About 85–90% of the asymptotically observed mesons are already free at chemical freeze-out. The energy dependence of the $N(1535)$ resonance contribution is comparable to that of the pion contribution from $\Delta(1232)$ decays (see also Fig. 9). For pions as well as for η mesons a trend towards larger contributions from resonance decays is visible in the heavier systems.

D. Time Order of Chemical and Thermal Freeze-out

In a sudden freeze-out scenario the temperature of an equilibrated hadron gas at thermal freeze-out is characterized by the momentum spectra of the emitted particles. The experimental spectra, however, may be modified by resonance decays and, in particular in heavy systems, by the rescattering of particles off spectator material. In addition, energy transferred into collective flow reduces the temperature of the system. Thus, in order to extract the freeze-out temperature T_{th} from the spectral shapes, further assumptions have to be made leading to model–dependent results. Nevertheless, the meson spectra of the present data base do provide a valuable consistency check for the chemical freeze-out analysis in the sense that the different model temperatures are subject to constraints due to the time order of chemical and thermal freeze-out.

As an example we consider the impact–parameter inclusive transverse–mass spectra of

π^0 and η mesons presented in Fig. 3. The spectra can be described reasonably well by exponential distributions, provided one excludes the low transverse masses from the fit. For all three collision systems the Boltzmann parameters T_B , which reflect the temperature T_{th} of the fireball at thermal freeze-out in case of vanishing collective flow, agree with the corresponding chemical freeze-out temperatures T_c . A similar quality of agreement is observed for Ar + Ca at 1.5A GeV, see Tab. IV. At the lower beam energies of 1.0A and 0.8A GeV the experimental situation for T_B seems unclear at present, except for the heavy systems Kr + Zr and Au + Au. In Au + Au at 0.8A GeV we have $T_B > T_c$ at the 1σ level, while at 1.0A GeV the Boltzmann temperatures in both systems are significantly higher than the corresponding chemical freeze-out temperatures, see Tab. IV.

The absence of a low- m_t enhancement in the C + C spectrum of Fig. 3 is remarkable. To the extent that rescattering can be assumed negligible, the light C + C system should show the expected influence of resonance decay. Instead, a perfectly exponential behavior is observed over the full m_t range, although pions from resonance decay do comprise 40% of the total pion intensity (see Fig. 10). Consequently, the onset of the low- m_t enhancement visible in the Ca + Ca and Ni + Ni cases of Fig. 3 probably has to be attributed to rescattering in spectator material.

Collective flow affects the meson spectra. The point is, that one has to know the underlying flow profile in order to analyze a given spectral shape. For the present analysis we have chosen the blast model proposed by Siemens and Rasmussen [39]. In this model, the fireball in thermal equilibrium is assumed to expand isotropically. All particles in the fireball share a common temperature T_{SR} and have a common radial-flow velocity β_{SR} . The modification of the spectra compared to pure Boltzmann distributions becomes more significant the heavier the considered particle species is. Since pions and η mesons have low masses their spectra are not very sensitive to the radial-flow velocity. Therefore, a fit to the mesonic transverse-mass spectra considering both T_{SR} and β_{SR} as free parameters would determine the freeze-out parameters only with large uncertainties. To avoid this situation, we exploit the fact that for the present range of collision systems β_{SR} is known to have values

between 0.25 and 0.35 in accord with the systematics of radial flow velocities measured for heavier particles ($A=1$ to 4) in central collisions as quoted in [40]. Thus only T_{SR} is treated as a fit parameter while β_{SR} is kept constant. In the π^0 cases we furthermore restrict the fit to $m_t \geq 400$ MeV as was done for the Boltzmann fits. Under these conditions the π^0 and η spectra can be described within the Siemens–Rasmussen model for all beam energies and target–projectile combinations. In general, the extracted temperatures T_{SR} are 10–20% smaller than the corresponding Boltzmann temperatures T_B , see Fig. 11. The actual reduction is correlated with the magnitude of β_{SR} chosen in the fit, with T_{SR} decreasing for increasing β_{SR} .

Thermal freeze–out does not occur before chemical freeze–out and, therefore, the thermal freeze–out temperature T_{th} cannot be larger than T_c . The available midrapidity spectra of the π^0 and η mesons do support this conjecture. If one neglects radial flow, the spectral shapes observed in the light and intermediate–mass systems provide inverse–slope parameters which are in accord with the chemical freeze–out temperatures T_c derived from the particle yields. Taking radial flow into account results in slightly lower temperatures at thermal freeze–out compared to chemical freeze–out, indicative of cooling as the system develops in time. The meson spectra observed in the heavy systems Kr + Zr and Au + Au, in particular, do require the inclusion of flow in order to achieve consistency ($T_c \geq T_{th}$) between thermal and chemical freeze–out temperatures.

E. Chemical Freeze–out Curve for Hadronic Matter

Fig. 12 shows our results within a schematic phase diagram of hadronic matter, together with other data points obtained from particle–production experiments at higher energies [10,11]. In contrast to the AGS and SPS results the chemical freeze–out parameters deduced at SIS energies are far below the expected phase boundary between hadron gas and quark–gluon plasma. For zero chemical potential the critical temperature is constrained by lattice QCD calculations. For finite values of μ_B the phase boundary can be approximated in a

simple model by equating chemical potential and pressure in the hadronic phase and in an idealized quark–gluon plasma [11]. It has recently been noticed by Cleymans and Redlich that, within their hadron–gas model, the chemical freeze–out curve corresponds to an average energy per hadron of 1 GeV [41]. The resulting curve is shown in Fig. 12 as a solid line which is in close agreement with the deduced freeze–out parameters.

At SIS energies thermal and chemical freeze–out seem to nearly coincide. In contrast, at SPS beam energies the freeze–out parameters clearly indicate that thermal freeze–out reflects a later stage of the collision as significantly lower temperatures compared to chemical freeze–out are deduced [42].

VI. SUMMARY

The inclusive neutral–pion and η –meson yields measured in symmetric collisions of light, intermediate–mass, and heavy nuclei near midrapidity in the energy range from $0.8A$ GeV to $2.0A$ GeV are consistent with the formation of a hadronic fireball in chemical equilibrium, as described by an isospin–symmetric ideal hadron gas. With increasing bombarding energy the baryochemical potential μ_B decreases from 800 MeV to 650 MeV while simultaneously the temperature T_c increases from 55 MeV to 90 MeV. Concerning the system–size dependence, we find that μ_B grows with increasing mass of the projectile–target combination while T_c remains about constant. The centrality dependence of μ_B and T_c has been investigated in the system Au + Au at $0.8A$ GeV. Here the η/π^0 ratio is expected to be most susceptible to the impact parameter, both because of the large mass of the system and because of the low incident beam energy. No centrality dependence is observed.

Apart from the moderate system size dependence, the freeze–out parameters μ_B and T_c completely characterize the system. Given μ_B and T_c one can calculate the hadrochemical composition of the fireball. While at $0.8A$ GeV beam energy only 2–3% of the nucleons are excited to resonance states at chemical freeze–out, this fraction increases to about 15% at $2.0A$ GeV bombarding energy. According to transport–model calculations, this resonance

content at freeze-out implies a resonance density in the high-density phase of the collision of about normal nuclear matter density, thus justifying the term resonance matter for the specific state of hadronic matter created in heavy-ion collisions at SIS energies. In the meson sector of our model about 50% of all asymptotically observed pions are still bound in resonance states at chemical freeze-out, while only about 10% of the final-state η mesons are bound at that moment.

In contrast to the particle yields, which convey the status at chemical freeze-out, the shapes of the related transverse-mass spectra do reflect thermal freeze-out. After proper allowance for radial flow the slope parameters observed for the midrapidity spectra of the neutral mesons correspond to thermal freeze-out temperatures which are equal to or slightly lower than the chemical freeze-out temperatures. In contrast to ultrarelativistic collisions studied at the SPS, chemical and thermal freeze-out thus seem to occur almost simultaneously at SIS energies as is also observed for heavy-ion collisions at the AGS.

Particle yields and spectral shapes reflect only two facets of the very complex process of a relativistic nucleus-nucleus collision. With these observables alone it is not possible to decide whether chemical equilibrium is actually reached during any stage of such a collision. In fact, the observation that for the heavy collision systems the agreement between data and hadron-gas model is not as good as for the light systems can be seen as one indication that physics beyond equilibrium concepts may still be visible in the final state of relativistic nucleus-nucleus collisions around 1A GeV.

ACKNOWLEDGMENTS

The extensive data base on neutral-meson production in heavy-ion collisions as accumulated by the TAPS collaboration has been instrumental for this study. It is a pleasure to acknowledge helpful discussions with many colleagues, in particular with P. Braun-Munzinger, J. Cleymans, H. Oeschler, K. Redlich, and P. Senger. One of us (R.A.) is supported by the A. v. Humboldt Foundation as an F. Lynen fellow.

REFERENCES

- * Electronic address: R.Averbeck@gsi.de
Present address: Department of Physics and Astronomy,
State University of New York at Stony Brook,
Stony Brook, New York 11794-3800, USA
- [1] R. Stock: Phys. Rep. 135 (1986) 259 and references therein
- [2] W. Cassing et al.: Phys. Rep. 188 (1990) 363
- [3] J. Aichelin: Phys. Rep. 202 (1991) 233
- [4] T. Maruyama et al.: Nucl. Phys. A 573 (1994) 653
- [5] S.A. Bass et al.: Phys. Rev. C 51 (1995) 3343
- [6] W. Ehehalt et al.: Phys. Rev. C 47 (1993) 2467
- [7] V. Metag: Prog. Part. Nucl. Phys. 30 (1993) 75
- [8] U. Mosel, V. Metag: Phys. Bl. 49 (1993) 426
- [9] J. Cleymans and H. Satz: Z. Phys. C 57 (1993) 135
- [10] P. Braun-Munzinger et al.: Phys. Lett. B 344 (1995) 43
- [11] P. Braun-Munzinger et al.: Phys. Lett. B 365 (1996) 1
- [12] J. Sollfrank: J. Phys. G 23 (1997) 1903
- [13] B. Hong et al.: Phys. Rev. C 57 (1998) 244
- [14] J. Cleymans et al.: Phys. Rev. C 57 (1998) 3319
- [15] J. Cleymans et al.: Phys. Rev. C 59 (1999) 1663
- [16] A.R. Wolf et al.: Phys. Rev. Lett. 80 (1998) 5281
- [17] F.-D. Berg et al.: Phys. Rev. Lett. 72 (1994) 977

- [18] O. Schwalb et al.: Phys. Lett. B 321 (1994) 20
- [19] M. Appenheimer: PhD thesis, University Gießen, 1997
- [20] R. Averbeck et al.: Z. Phys. A 359 (1997) 65
- [21] A. Marín et al.: Phys. Lett. B 409 (1997) 77
- [22] G. Martínez et al.: Phys. Rev. Lett. 83 (1999) 1538
- [23] P. Vogt: PhD thesis, University Groningen, 1998
- [24] C. Müntz et al.: Z. Phys. A 357 (1997) 399
- [25] D. Pelte et al.: Z. Phys. A 357 (1997) 215
- [26] R. Hagedorn: Rivista del Nuovo Cimento, vol. 6, no. 10, 1983
- [27] J. Stachel and G.R. Young: Ann. Rev. Nucl. Part. Sci. 42 (1992) 537
- [28] S.A. Bass et al.: Phys. Rev. Lett. 71 (1993) 1144
- [29] S. Teis et al.: Z. Phys. A 356 (1997) 421
- [30] R. Balian and C. Bloch: Ann. Phys. 60 (1970) 401
- [31] H.R. Jaqaman et al.: Phys. Rev. C 29 (1984) 2067
- [32] D.E. Groom et al., Particle Data Group: Eur. Phys. J. C 15 (2000) 1
- [33] J.H. Koch et al.: Ann. Phys. (N.Y.) 154 (1984) 99
- [34] B. Krusche et al.: Phys. Rev. Lett. 74 (1995) 3736
- [35] H. Pöppel: PhD thesis, University Marburg, 1993
- [36] S. Nagamiya et al.: Phys. Rev. C 24 (1981) 971
- [37] D.E. Groom et al., Particle Data Group: Eur. Phys. J. C 15 (2000) 195
- [38] H. Weber: Diploma thesis, University Frankfurt, 1996

[39] P.J. Siemens and J.O. Rasmussen: Phys. Rev. Lett. 42 (1979) 880

[40] N. Herrmann: Nucl. Phys. A 610 (1996) 49c

[41] J. Cleymans and K. Redlich: Nucl. Phys. A 661 (1999) 379c

[42] R. Stock: Nucl. Phys. A 630 (1998) 535c

FIGURES

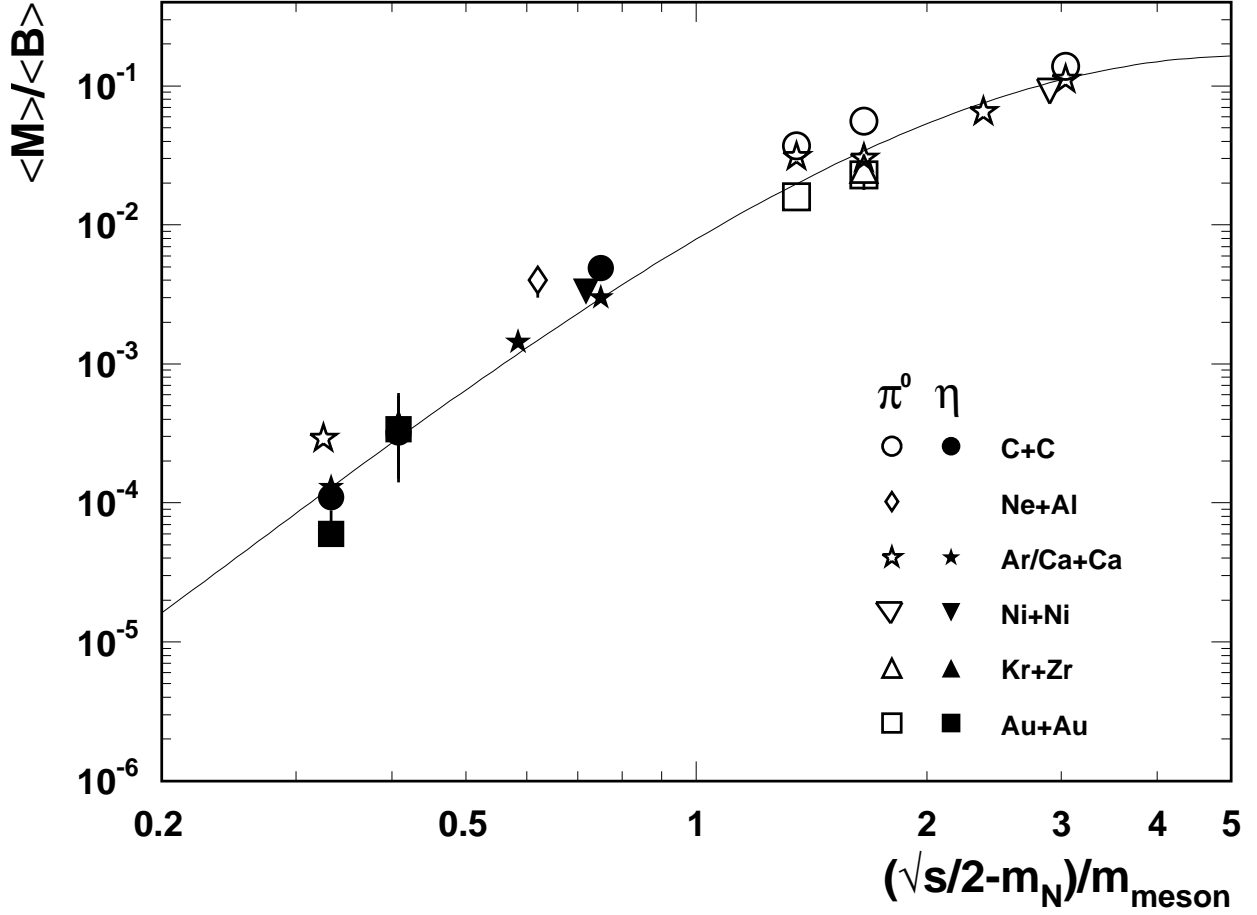


FIG. 1. Average π^0 and η -meson multiplicities per average number of participants in symmetric nucleus–nucleus collisions as a function of the energy available per baryon normalized to the mass of the respective meson. The data are taken from [16–23]. The curve represents a fit to the data and is given by the polynomial expression $\log(\langle M \rangle / \langle B \rangle) = -2.102 + (3.25 - (1.405 + 0.785 \log x) \log x) \log x$, where x is the normalized meson–specific energy available.

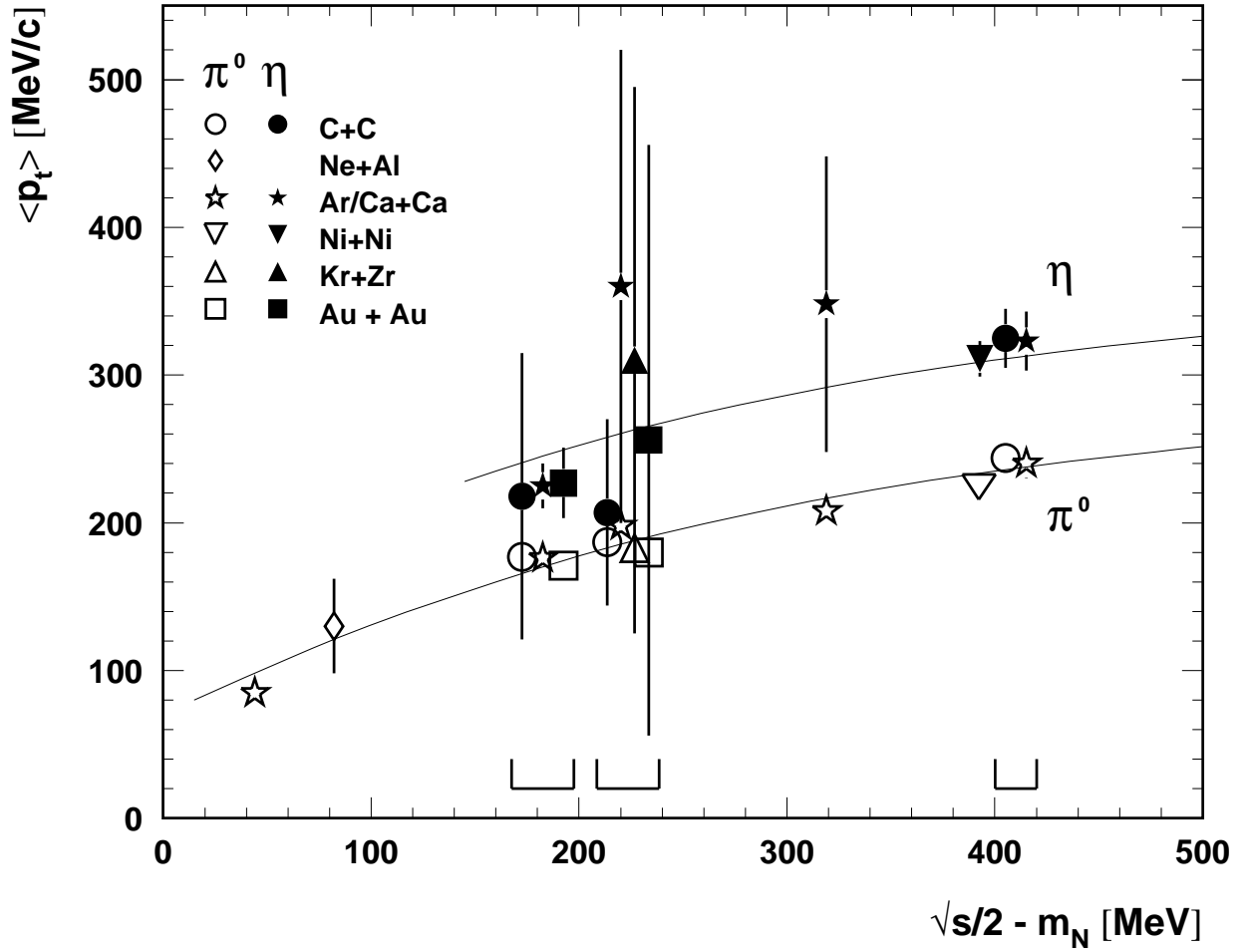


FIG. 2. Average π^0 and η -meson transverse momenta measured in narrow rapidity intervals around midrapidity as a function of the energy available per baryon. The data are taken from the same experiments as listed in Fig. 1. The data points at available energies of 182 MeV (0.8A GeV beam energy), 223 MeV (1.0A GeV), and 410 MeV (2.0A GeV) are slightly shifted in energy with respect to their nominal position (center of brackets) to make the error bars of the η momentum visible. With the exception of Ne + Al the error bars for the π^0 momentum are smaller than the symbol size. Parallel lines interpolating the π^0 and η data, respectively, are drawn to guide the eye.

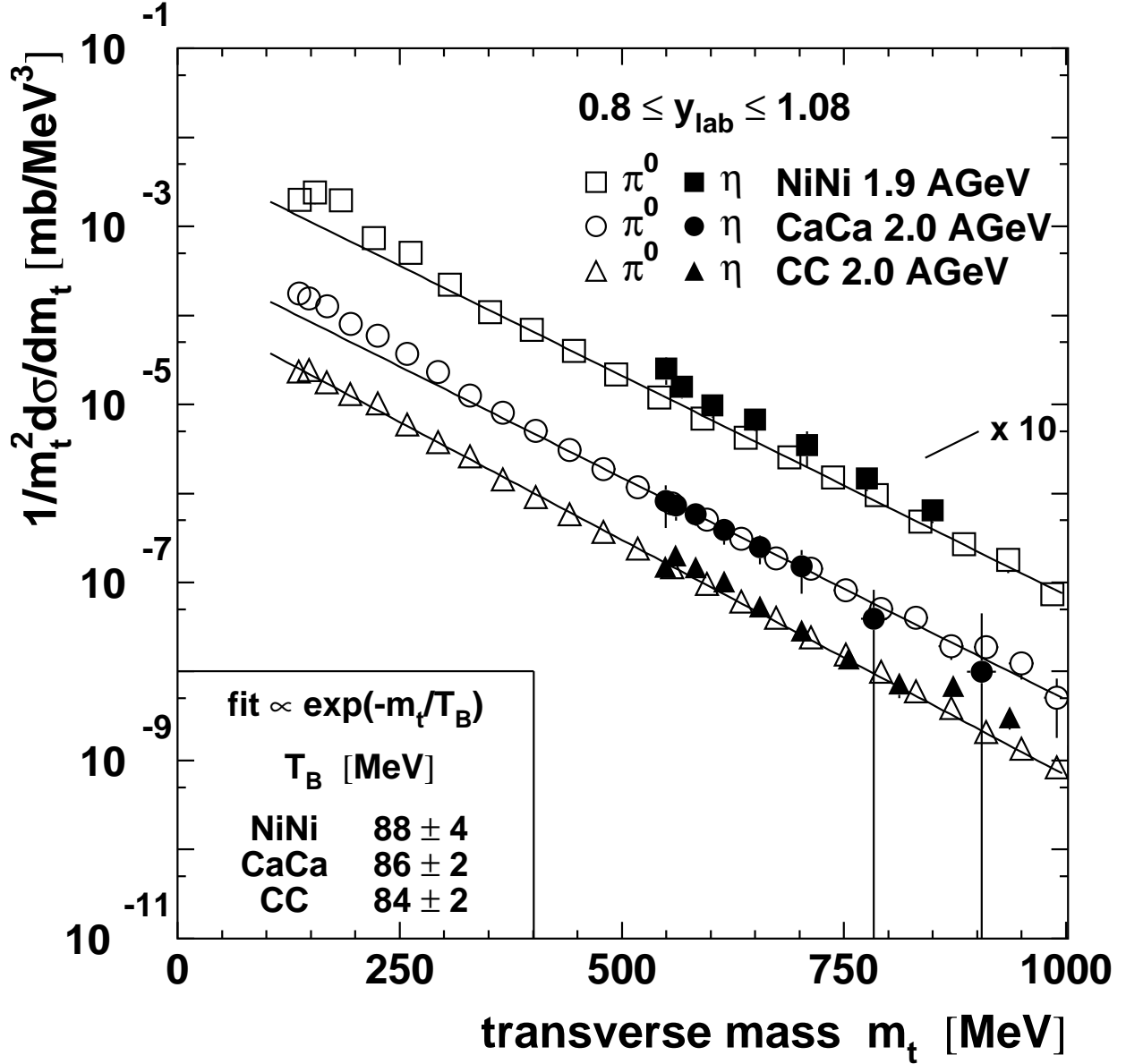


FIG. 3. Impact-parameter inclusive transverse-mass spectra of π^0 and η -mesons as observed in the systems C + C [20] and Ca + Ca [23] at 2.0A GeV beam energy and in Ni + Ni at 1.9A GeV [19]. The distributions are divided by the square of the transverse mass. In this representation midrapidity particles from a thermal source are expected to exhibit a purely exponential spectrum. The solid lines represent Boltzmann fits (see Eq. 1) to the π^0 data for $m_t \geq 400$ MeV.

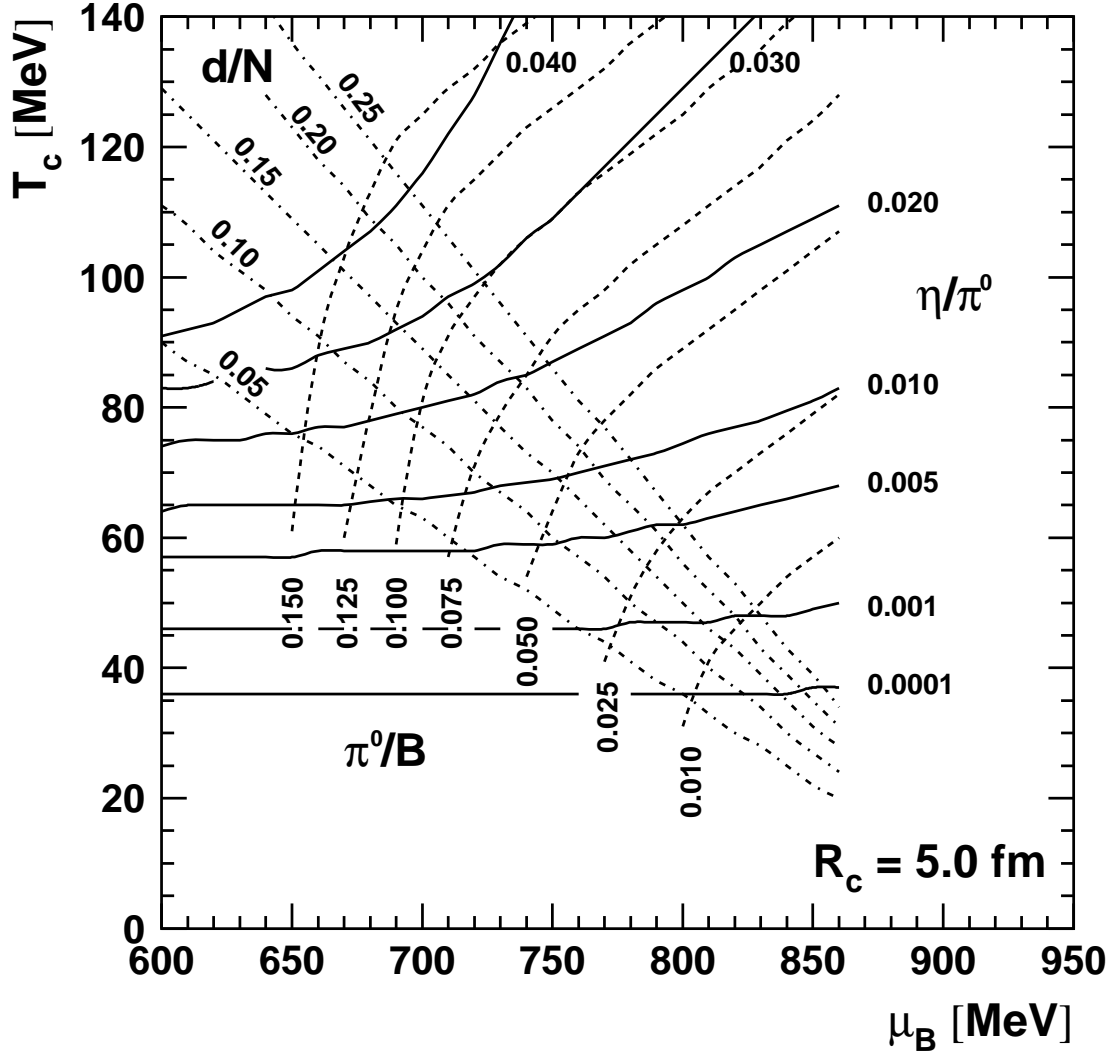


FIG. 4. Freeze-out lines in the μ_B, T_c -plane for selected values of the particle ratios π^0/B , η/π^0 , and d/N . The diagram corresponds to a fixed size of the system with the consequence that the baryon density $\rho_B(\mu_B, T_c)$ changes. Representative densities are $\rho_B(650 \text{ MeV}, 70 \text{ MeV})=0.053 \rho_0$, $\rho_B(650 \text{ MeV}, 100 \text{ MeV})=0.469 \rho_0$, $\rho_B(800 \text{ MeV}, 80 \text{ MeV})=1.197 \rho_0$, and $\rho_B(800 \text{ MeV}, 50 \text{ MeV})=0.125 \rho_0$, where ρ_0 is the nuclear ground-state density $\rho_0 = 0.168 \text{ fm}^{-3}$.

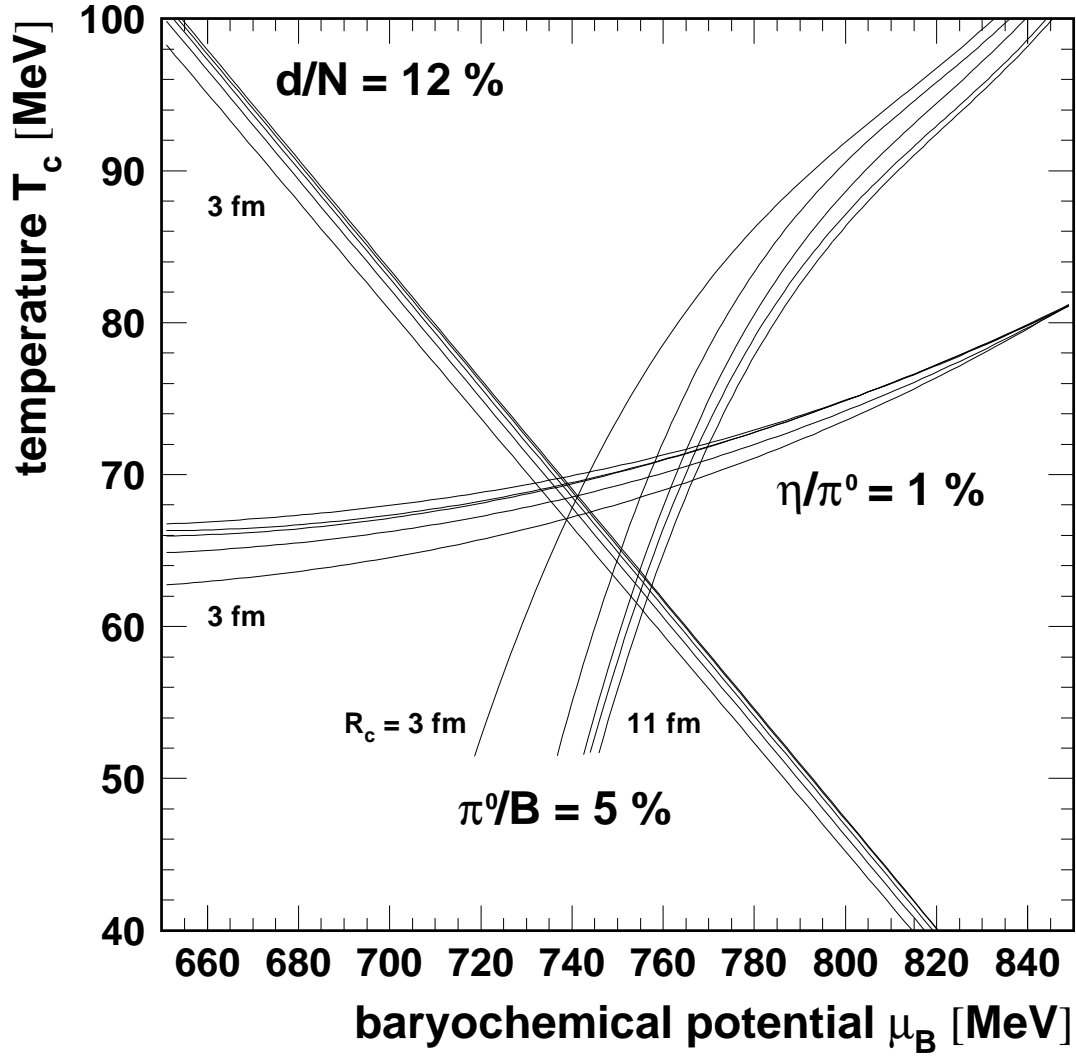


FIG. 5. Freeze-out lines in the μ_B, T_c -plane for selected values of the freeze-out radius R_c . The diagram corresponds to fixed particle ratios π^0/B , η/π^0 , and d/N , while R_c varies in equidistant steps from 3 fm to 11 fm as indicated.

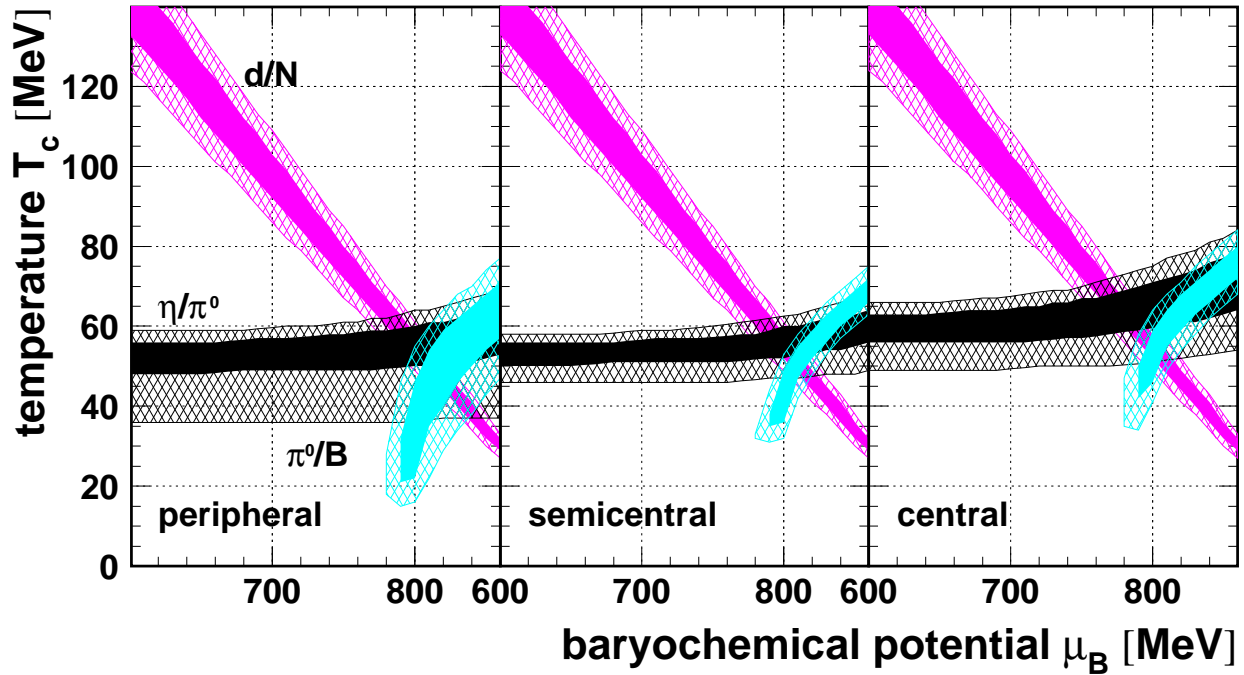


FIG. 6. Determination of the chemical freeze-out parameters in the system Au + Au at 0.8A GeV beam energy for peripheral ($\langle B \rangle = 40 \pm 10$, left), semicentral ($\langle B \rangle = 227 \pm 20$, middle), and central collisions ($\langle B \rangle = 345 \pm 25$, right). For given impact parameter the particle ratios π^0/B , η/π^0 , and d/N define three bands, shown in different greyscales, in the μ_B, T_c -plane. The solid (hatched) bands reflect 1σ (2σ) intervals in the experimental uncertainties. The freeze-out parameters are determined by the overlap of the three bands.

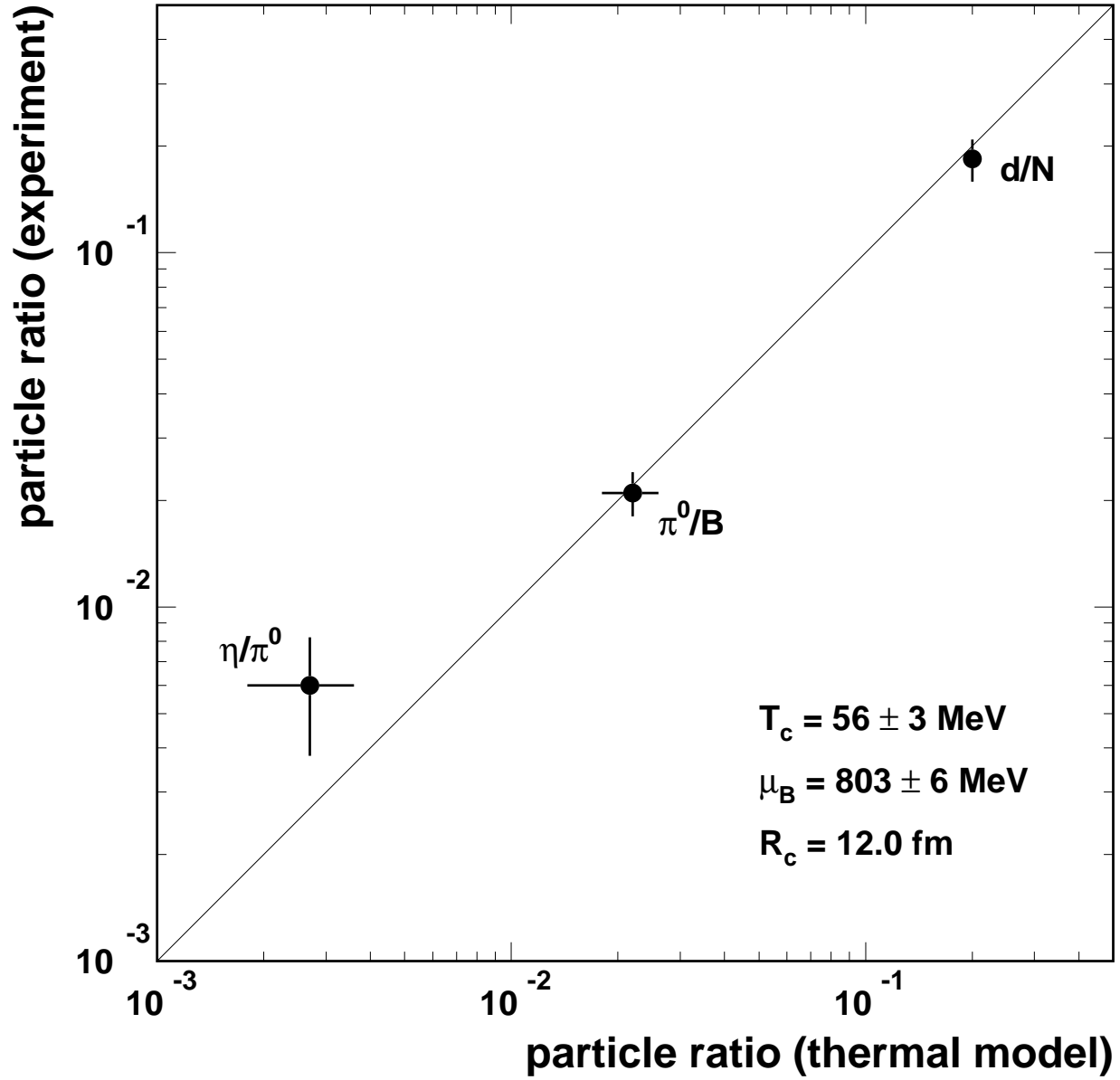


FIG. 7. Comparison between experimental particle ratios and ratios as calculated from the baryochemical potential μ_B and the temperature T_c at freeze-out. The case shown corresponds to central Au + Au collisions at 0.8A GeV with baryon number $\langle B \rangle = 345 \pm 25$. R_c is the freeze-out radius.

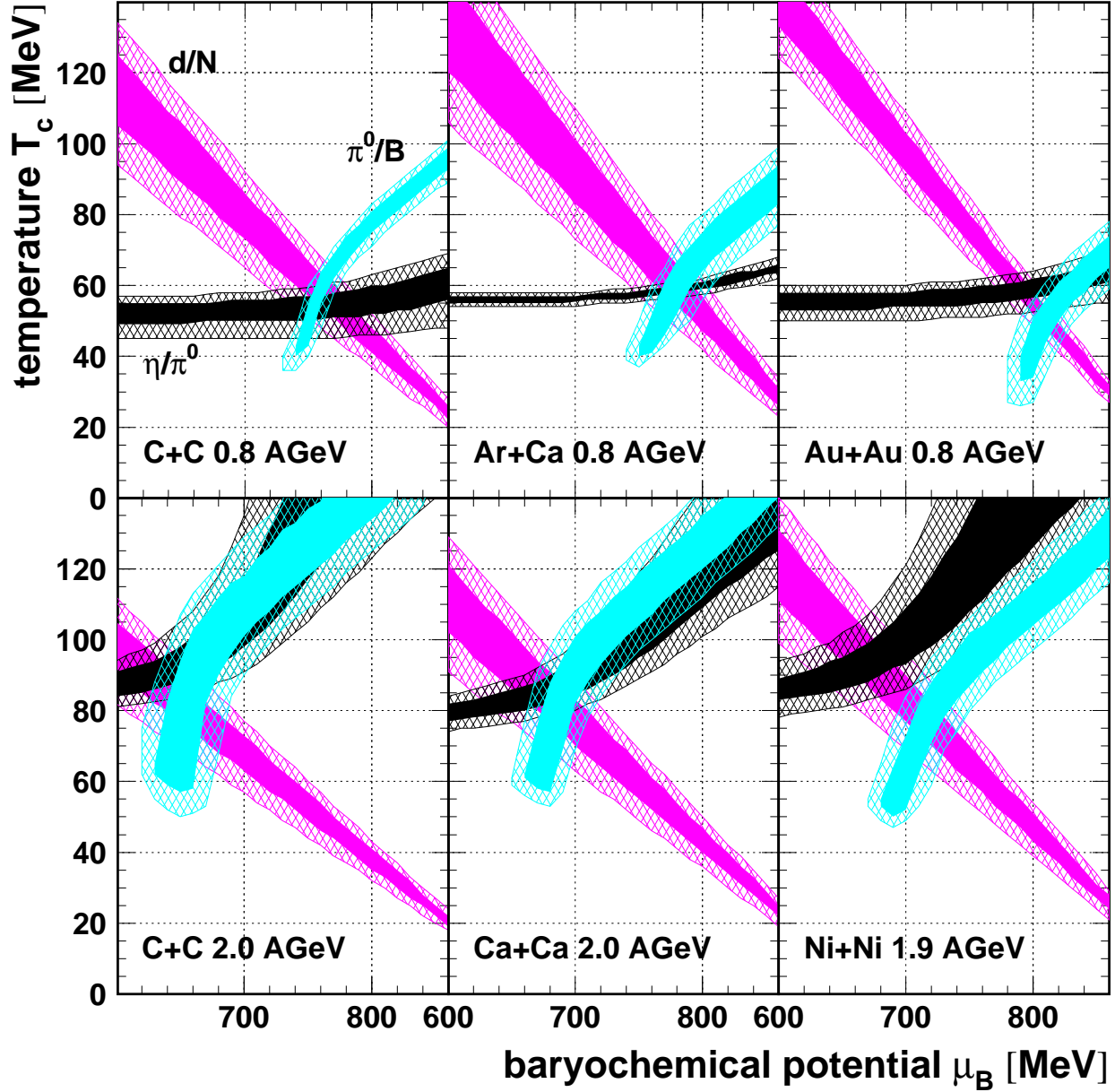


FIG. 8. Determination of the chemical freeze-out parameters T_c and μ_B . For given system and beam energy the particle ratios π^0/B , η/π^0 , and d/N define three bands, distinguished by different greyscales, in the μ_B, T_c -plane. The solid (hatched) bands reflect 1σ (2σ) intervals in the experimental uncertainties. The freeze-out parameters are determined by the overlap of the three bands. The individual panels show the solutions obtained for the lightest, an intermediate-mass, and the heaviest system studied at the lowest and highest beam energies, respectively.

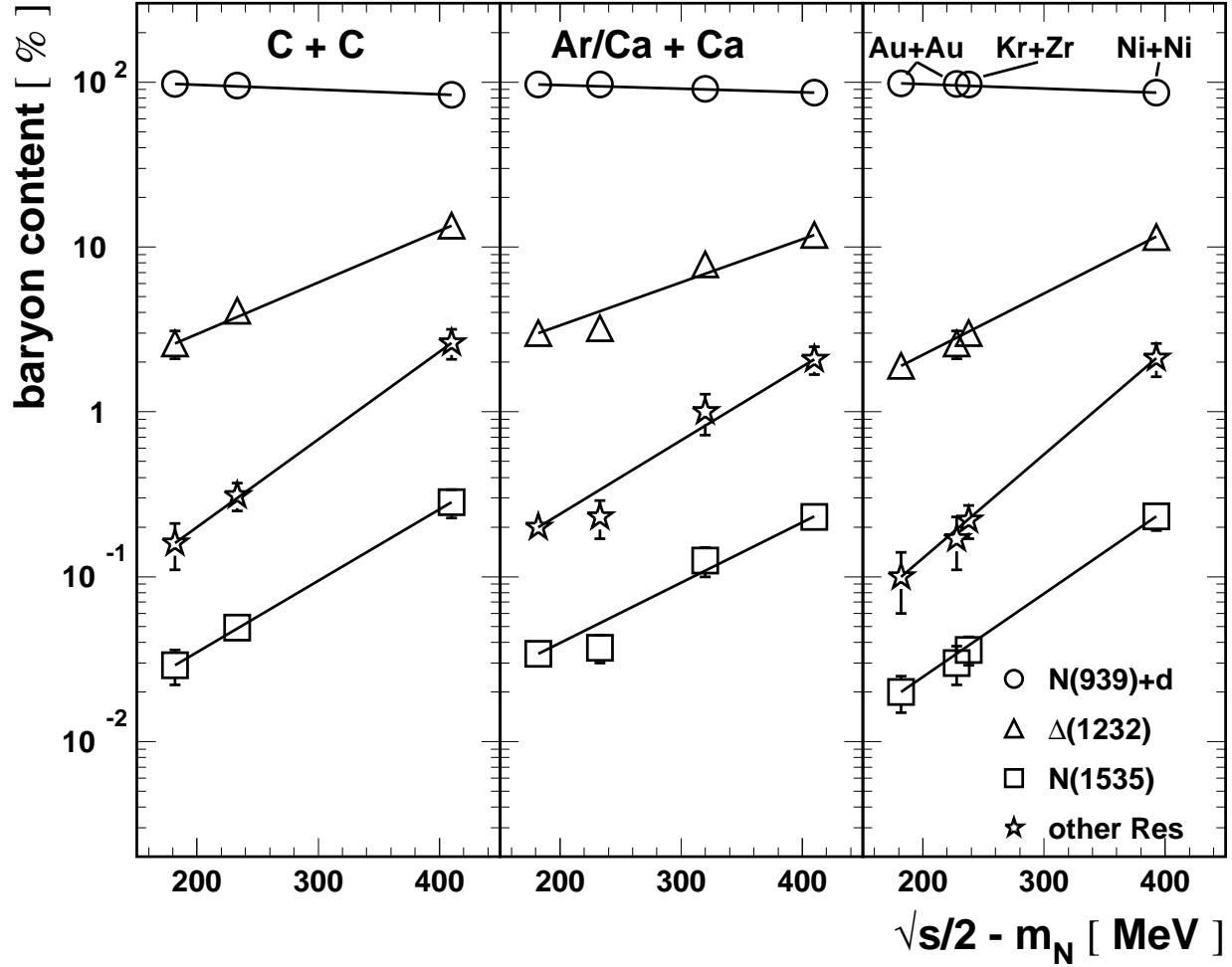


FIG. 9. Baryon content at chemical freeze-out in the hadron-gas model. The relative contributions to the total baryon number from nucleons and deuterons, $\Delta(1232)$ resonances, $N(1535)$ resonances, and the sum of all remaining Δ and N resonances are plotted as a function of the energy available per baryon. The three panels show from left to right the results obtained for light, intermediate-mass, and heavy systems. The error bars reflect the uncertainty in the freeze-out parameters μ_B and T_c (see Tab. IV). Straight lines are drawn to guide the eye.

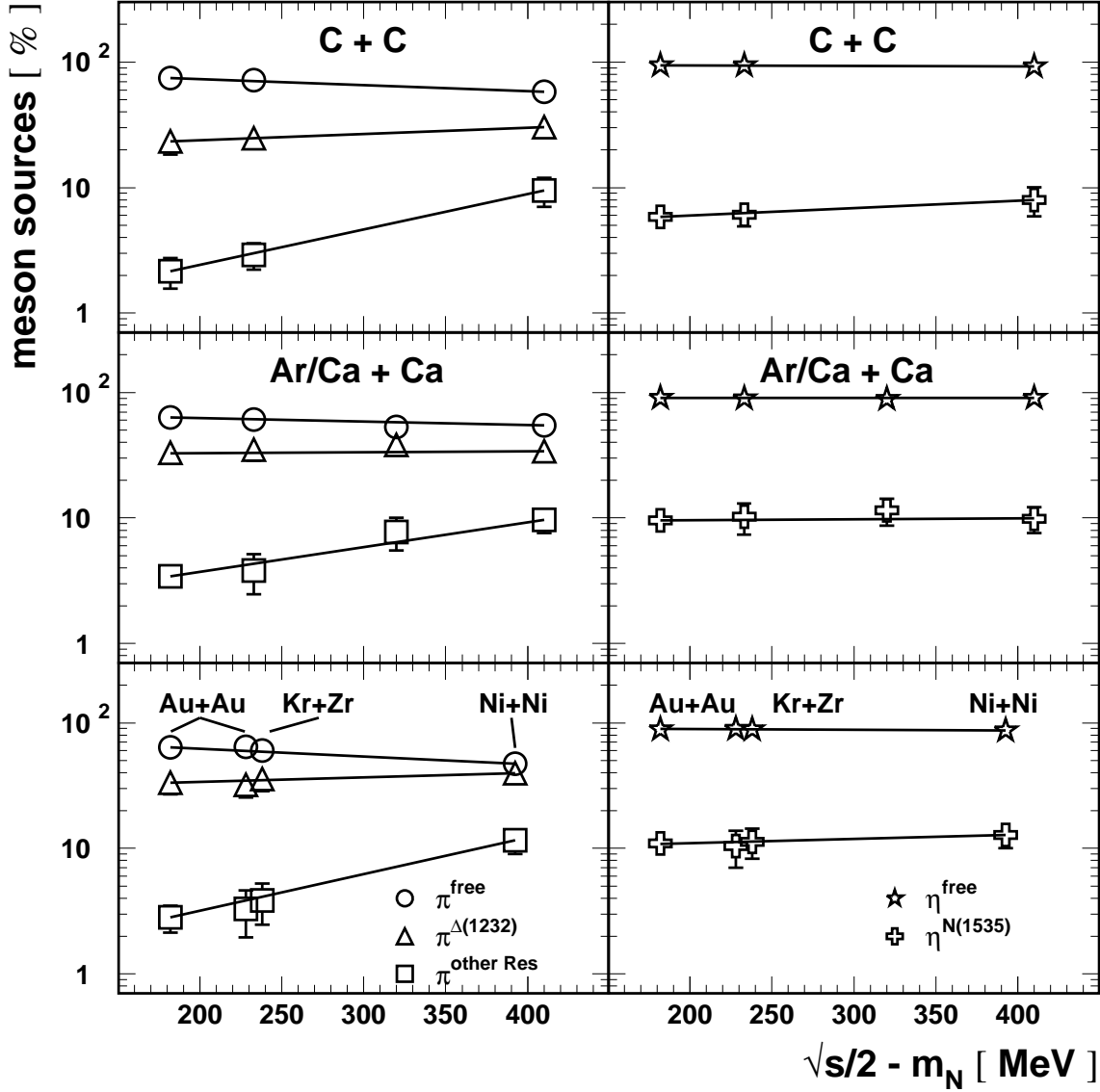


FIG. 10. Pion (left) and η meson sources (right) at chemical freeze-out in the hadron-gas model. The mesons are either present as free particles or still bound in resonance states. The corresponding relative contributions are shown as a function of the energy available per baryon for light (top), intermediate-mass (middle), and heavy systems (bottom). The error bars reflect the uncertainty in the freeze-out parameters μ_B and T_c (see Tab. IV). Straight lines are drawn to guide the eye.

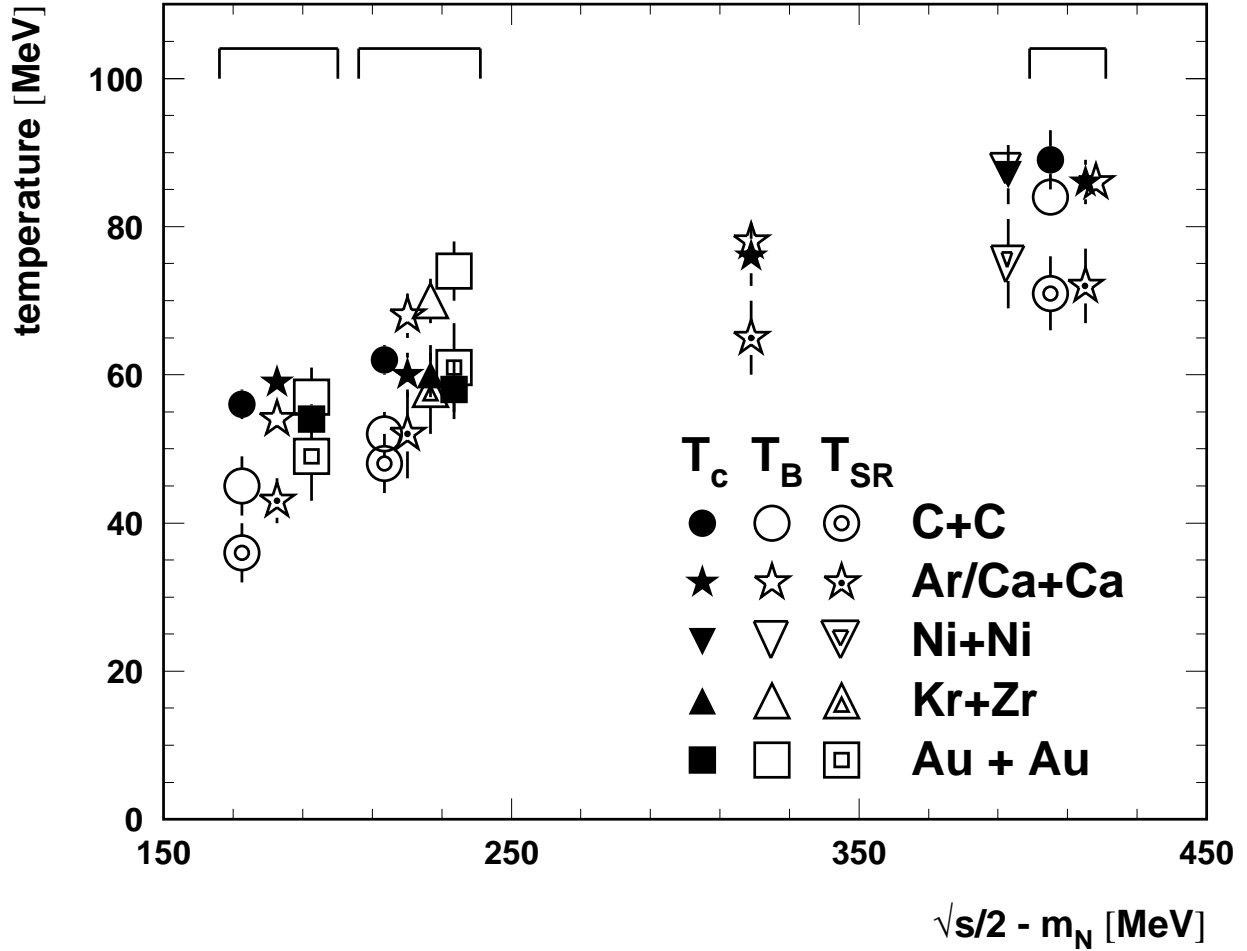


FIG. 11. Chemical (T_c) and model-dependent thermal (T_B and T_{SR}) freeze-out temperatures as a function of the energy available per baryon. The data points at 0.8A GeV, 1.0A GeV, and 2.0A GeV beam energy are slightly shifted in energy with respect to their nominal position (center of brackets).

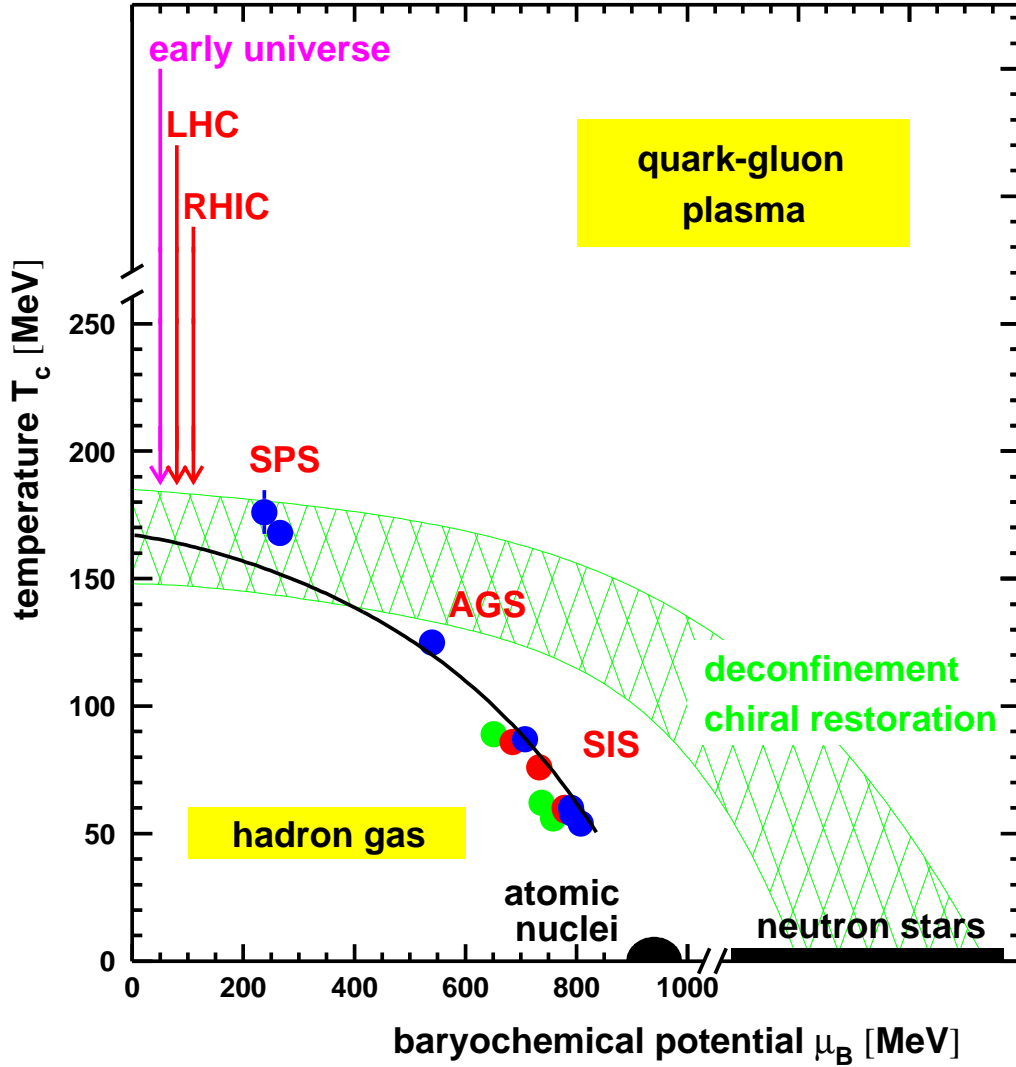


FIG. 12. Phase diagram of hadronic matter. The chemical freeze-out temperatures T_c are shown as a function of the corresponding baryochemical potentials μ_B as obtained from yield ratios of particles produced in nucleus-nucleus collisions at various incident energies. Results of the present work are plotted together with AGS and SPS results [10,11]. The grayscale of the SIS data points reflects the system size, i.e. light (dark) points correspond to light (heavy) systems. The solid curve (taken from Ref. [41]) approximates the curve for chemical freeze-out of hadronic matter. It corresponds to an average energy per hadron of 1 GeV in a hadron-gas model, while the crosshatched band indicates location and uncertainty of the boundary between a gas of hadrons and a plasma of gluons and deconfined quarks.

TABLES

TABLE I. Mean inclusive π^0 multiplicities $\langle M_{\pi^0} \rangle$ relative to the average number of participating nucleons $\langle B \rangle$ and mean inclusive η multiplicities $\langle M_\eta \rangle$ relative to $\langle M_{\pi^0} \rangle$ measured for various nucleus–nucleus collisions in the beam–energy range from $0.8A$ GeV to $2.0A$ GeV. The last column denotes interpolated mean deuteron multiplicities $\langle M_d \rangle$ relative to the mean nucleon multiplicity $\langle M_N \rangle$. The data for Kr + Zr and Au + Au (both at $1A$ GeV, see [18]) have been revised to account for the fact that the first–level trigger condition in effect in these measurements introduced a bias towards centrality.

E_{beam} [A GeV]	System	$\langle B \rangle$	$\frac{\langle M_{\pi^0} \rangle}{\langle B \rangle}$ [%]	$\frac{\langle M_\eta \rangle}{\langle M_{\pi^0} \rangle}$ [%]	$\frac{\langle M_d \rangle}{\langle M_N \rangle}$ [%]
0.8	C + C	6	3.7 ± 0.3	0.31 ± 0.11	11.3 ± 2.7
0.8	Ar + Ca	20	3.1 ± 0.5	0.41 ± 0.04	16.3 ± 3.9
0.8	Au + Au	125 ± 15	1.6 ± 0.3	0.38 ± 0.08	18.4 ± 2.5
1.0	C + C	6	5.6 ± 0.4	0.57 ± 0.14	10.6 ± 2.5
1.0	Ar + Ca	20	3.0 ± 0.3	1.3 ± 0.8	15.3 ± 3.7
1.0	Kr + Zr	79 ± 9	2.5 ± 0.7	1.3 ± 0.6	17.7 ± 2.3
1.0	Au + Au	164 ± 20	2.3 ± 0.5	1.4 ± 0.6	17.2 ± 2.3
1.5	Ar + Ca	20	6.5 ± 0.5	2.2 ± 0.4	12.7 ± 3.0
2.0	C + C	6	13.8 ± 1.4	3.6 ± 0.4	7.0 ± 1.7
2.0	Ca + Ca	20	11.1 ± 1.1	2.7 ± 0.3	10.2 ± 2.5
1.9	Ni + Ni	29	8.6 ± 0.9	3.3 ± 0.4	12.7 ± 2.8

TABLE II. Baryon resonances considered as constituents of the hadronic fireball. Given for each resonance are the nominal mass m_R , the total width Γ_R at m_R as well as the partial widths corresponding to the three decay modes considered in the present model. Values are taken from [32] (3- or 4-star status) with the exception of $\Delta(1232)$ [33] and $N(1535)$ [34].

resonance	mass m_R [MeV]	width Γ_R [MeV]	$\Gamma_{1\pi}/\Gamma_R$ [%]	$\Gamma_{2\pi}/\Gamma_R$ [%]	Γ_{η}/Γ_R [%]
$\Delta(1232)$	1232	110	100	0	0
$N(1440)$	1440	350	65	35	0
$N(1520)$	1520	120	55	45	0
$N(1535)$	1544	203	50	0	50
$\Delta(1600)$	1600	350	15	85	0
$\Delta(1620)$	1620	150	30	70	0
$N(1650)$	1650	150	80	20	0
$N(1675)$	1675	150	45	55	0
$N(1680)$	1680	130	65	35	0
$N(1700)$	1700	100	10	90	0
$\Delta(1700)$	1700	300	15	85	0
$N(1710)$	1710	100	15	85	0
$N(1720)$	1720	150	20	80	0

TABLE III. Particle ratios and chemical freeze-out parameters for peripheral, semicentral, and central collisions in the system Au + Au at 0.8A GeV. The impact parameter was selected according to the number of participating nucleons $\langle B \rangle$ given in the first row. The next entries denote the meson ratios ($\langle M_{\pi^0} \rangle / \langle B \rangle$, $\langle M_{\eta} \rangle / \langle M_{\pi^0} \rangle$), the inclusive deuteron/nucleon ratio $\langle M_d \rangle / \langle M_N \rangle$, and the freeze-out radius R_c . The subsequent rows show the freeze-out parameters μ_B and T_c together with the resulting baryon density ρ_B relative to the nuclear ground-state density $\rho_0 = 0.168 \text{ fm}^{-3}$. The values are determined by χ^2 minimization, the uncertainties represent 1σ standard deviations as evaluated from the size of the error ellipse of the μ_B, T_c pair at $\chi^2 = \chi_{min}^2 + 1$.

	peripheral	semicentral	central
$\langle B \rangle$	40 ± 10	227 ± 20	345 ± 25
$\langle M_{\pi^0} \rangle / \langle B \rangle$ [%]	1.3 ± 0.4	1.6 ± 0.2	2.1 ± 0.3
$\langle M_{\eta} \rangle / \langle M_{\pi^0} \rangle$ [%]	0.27 ± 0.13	0.29 ± 0.10	0.60 ± 0.22
$\langle M_d \rangle / \langle M_N \rangle$ [%]	18.4 ± 2.5 (inclusive)		
R_c [fm]	6.5	11.0	12.0
μ_B [MeV]	812 ± 5	812 ± 5	803 ± 6
T_c [MeV]	51 ± 2	52 ± 2	56 ± 3
ρ_B / ρ_0	0.21 ± 0.07	0.23 ± 0.08	0.28 ± 0.09
χ_{min}^2	0.88	1.50	2.93

TABLE IV. Chemical freeze-out parameters μ_B and T_c for the various systems investigated, together with the resulting baryon densities ρ_B . The values are determined by χ^2 minimization, uncertainties represent 1σ standard deviations as evaluated from the size of the error ellipse of the μ_B, T_c pair at $\chi^2 = \chi_{min}^2 + 1$. Also given are the model-dependent thermal freeze-out temperatures T_B and T_{SR} as obtained from Boltzmann fits and within the blast model of Siemens and Rasmussen, respectively.

E_{beam} [A GeV]	System	chemical freeze-out					thermal freeze-out	
		R_c [fm]	μ_B [MeV]	T_c [MeV]	ρ_B/ρ_0	χ_{min}^2	T_B [MeV]	T_{SR} [MeV]
0.8	C + C	4.5	758 ± 5	56 ± 2	0.09 ± 0.03	0.36	45 ± 4	36 ± 4
0.8	Ar + Ca	5.5	780 ± 7	59 ± 1	0.19 ± 0.05	0.10	54 ± 2	43 ± 3
0.8	Au + Au	8.5	808 ± 5	54 ± 2	0.27 ± 0.08	5.90	57 ± 4	49 ± 6
1.0	C + C	4.5	737 ± 5	62 ± 2	0.10 ± 0.03	1.05	52 ± 3	48 ± 4
1.0	Ar + Ca	5.0	779 ± 7	60 ± 3	0.21 ± 0.08	1.14	68 ± 3	52 ± 6
1.0	Kr + Zr	7.5	790 ± 7	60 ± 3	0.27 ± 0.09	2.30	70 ± 3	58 ± 6
1.0	Au + Au	9.5	792 ± 7	58 ± 4	0.27 ± 0.09	3.95	74 ± 4	61 ± 6
1.5	Ar + Ca	4.5	733 ± 7	76 ± 4	0.30 ± 0.10	4.46	78 ± 2	65 ± 5
2.0	C + C	3.5	651 ± 8	89 ± 4	0.21 ± 0.07	2.39	84 ± 2	71 ± 5
2.0	Ca + Ca	4.5	685 ± 9	86 ± 3	0.30 ± 0.08	0.96	86 ± 2	72 ± 5
1.9	Ni + Ni	4.5	707 ± 9	87 ± 4	0.43 ± 0.16	8.06	88 ± 4	75 ± 6